

1 **Short Communication**

2 **Dysregulation in mTOR/HIF-1 signaling identified by proteo-transcriptomics of SARS-**  
3 **CoV-2 infected cells**

4  
5 Sofia Appelberg<sup>1#</sup>, Soham Gupta<sup>2#</sup>, Anoop T Ambikan<sup>2</sup>, Flora Mikaeloff<sup>2</sup>, Ákos Végvári<sup>3</sup>, Sara  
6 Svensson Akusjärvi<sup>2</sup>, Rui Benfeitas<sup>4</sup>, Maïke Sperk<sup>2</sup>, Marie Ståhlberg<sup>3</sup>, Shuba Krishnan<sup>2</sup>, Kamal  
7 Singh<sup>2,5</sup>, Josef M. Penninger<sup>6,7</sup>, Ali Mirazimi<sup>1,2,8\*</sup>, Ujjwal Neogi<sup>2,5,9\*</sup>

8  
9 <sup>1</sup>Public Health Agency of Sweden, Solna, Sweden

10 <sup>2</sup>Division of Clinical Microbiology, Department of Laboratory Medicine, Karolinska Institute,  
11 ANA Futura, Campus Flemingsberg, Stockholm, Sweden.

12 <sup>3</sup>Division of Chemistry I, Department of Medical Biochemistry and Biophysics, Karolinska  
13 Institutet, Stockholm, Sweden

14 <sup>4</sup>National Bioinformatics Infrastructure Sweden (NBIS), Science for Life Laboratory, Department  
15 of Biochemistry and Biophysics, Stockholm University, S-10691 Stockholm, Sweden

16 <sup>5</sup>Department of Molecular Microbiology and Immunology and the Bond Life Science Center,  
17 University of Missouri, Columbia, MO 65211, USA

18 <sup>6</sup>Institute of Molecular Biotechnology of the Austrian Academy of Sciences, Dr. Bohr-Gasse 3,  
19 1030 Vienna, Austria.

20 <sup>7</sup>Department of Medical Genetics, Life Science Institute, University of British Columbia,  
21 Vancouver, V6T 1Z3, British Columbia, Canada.

22 <sup>8</sup>National Veterinary Institute, Uppsala, Sweden

23 <sup>#</sup>Equal contribution

24 <sup>\*</sup>Corresponding Authors: Ali Mirazimi ([ali.mirazimi@folkhalsomyndigheten.se](mailto:ali.mirazimi@folkhalsomyndigheten.se)), Ujjwal Neogi  
25 ([ujjwal.neogi@ki.se](mailto:ujjwal.neogi@ki.se))

26 **Abstract:**

27 How Severe Acute Respiratory Syndrome Coronavirus-2 (SARS-CoV-2) infections engage  
28 cellular host pathways and innate immunity in infected cells remain largely elusive. We  
29 performed an integrative proteo-transcriptomics analysis in SARS-CoV-2 infected HuH7 cells to  
30 map the cellular response to the invading virus over time. We identified four pathways, ErbB,  
31 HIF-1, mTOR and TNF signaling, among others that were markedly modulated during the course  
32 of the SARS-CoV-2 infection *in vitro*. Western blot validation of the downstream effector  
33 molecules of these pathways revealed a significant reduction in activated S6K1 and 4E-BP1 at 72  
34 hours post infection. Unlike other human respiratory viruses, we found a significant inhibition of  
35 HIF-1 $\alpha$  through the entire time course of the infection, suggesting a crosstalk between the SARS-  
36 CoV-2 and the mTOR/HIF-1 signaling. Further investigations are required to better understand  
37 the molecular sequelae in order to guide potential therapy in the management of severe COVID-  
38 19 patients.

39

40 **Introduction:**

41 The recent emergence of the coronavirus disease (COVID-19) pandemic caused by Severe Acute  
42 Respiratory Syndrome Coronavirus-2 (SARS-CoV-2) has created a public health emergency  
43 across the globe<sup>1-3</sup>. SARS-CoV-2, a single-stranded positive-sense RNA virus, is the seventh  
44 coronavirus that infects humans and belongs to the  $\beta$ -coronavirus family. Due to limited  
45 knowledge on molecular mechanisms of infection and pathogenesis there is currently no  
46 available vaccine or specific therapeutics to treat or prevent SARS-CoV-2 infection.

47 Understanding the viral dynamics and host responses to the virus are necessary to design better  
48 therapeutic strategies for COVID-19 patients. Within the short period of the pandemic, there are  
49 few reports (pre-prints) on different levels of omics data (transcriptomics, proteomics, and  
50 metabolomics) from cell culture infected with SARS-CoV-2 as well as patient material that  
51 aimed to elucidate potential mechanisms of the host immune response and disease pathogenesis  
52 of SARS-CoV-2. However, the steady state measurements fail to reveal the dynamic changes of  
53 the host and viral proteins during the course of the infection. Thus, the temporal changes in gene  
54 expression and protein synthesis in different phase of the infection has not yet been reported.

55 To provide a comprehensive assessment of the cellular response to SARS-CoV-2, we performed  
56 a time series integrative proteo-transcriptomics analysis in infected HuH7 cells ranging from the  
57 early phase of infection until the virus reached the ability to initiate cytopathic effect at ~72 hours  
58 post infection (hpi).

## 59 **Results:**

60 **Dynamics of the SARS-CoV-2 infection in HuH7 cell lines:** HuH7 cells were infected with  
61 SARS-CoV-2 at MOI 1.0<sup>4</sup>. Cells were collected at 24hpi, 48hpi and 72hpi and subjected to viral  
62 RNA quantification by quantitative PCR, transcriptomics by Illumina NextSeq550 and  
63 proteomics by tandem tag labeled mass spectrometry (TMT-MS). Transcriptomics, proteomics  
64 and proteo-transcriptomics data were further analyzed using in-depth bioinformatics (Fig 1a).  
65 qPCR targeting the E (envelope) gene of the SARS-CoV-2 identified a gradual increase in  
66 cellular viral RNA over time ( $p < 0.05$ , repeated measure ANOVA) (Fig 1b). RNAseq analysis  
67 detected viral RNA at all the time points; 24hpi, 48hpi and 72hpi (Fig 1c). The TMT-based  
68 quantitative proteomics also identified statistically significant increase ( $p < 0.05$ , repeated measure  
69 ANOVA) in SARS-CoV-2 proteins nucleocapsid (N), Membrane (M) and Spike (S) over time  
70 (Fig 1d). Thus, SARS-CoV-2 exposure of HuH7 cells results in effective infections that over time  
71 lead to enhanced viral RNA and viral protein production, required to assemble viral progeny.

72 **Host cellular response against SARS-CoV2 *in vitro*.** After having established effective SARS-  
73 CoV-2 infections, we assessed the cellular host response to the virus infection. We found that  
74 2622 genes and 1819 proteins were increased whereas 2856 genes and 1743 proteins were  
75 decreased significantly (false discovery rate  $< 0.05$ ) over the time despite distinct coverage (19997  
76 protein-coding genes vs 7757 proteins quantified). We next performed gene set enrichment  
77 analyses using the differentially expressed genes/proteins that are related to viral response,  
78 process and diseases (targeted analysis) obtained from Gene Ontology (GO), REACTOME and  
79 “Rare\_Diseases\_AutoRIF\_Gene\_Lists” library and mapped to KEGG (Human\_2019) terms.  
80 Figure 1e shows a heatmap of significantly enriched KEGG terms that are dysregulated in both  
81 our proteomics and transcriptomics analysis using for pairwise and time series analysis in  
82 uninfected and SARS-CoV-2 infected HuH7 cells. Of note, the downregulated genes did not  
83 identify any KEGG term with adjusted p value  $< 0.05$ . Among the most significantly upregulated  
84 pathways, mining both proteomics and transcriptomics data, were pathways associated with cell

85 proliferation and apoptosis, such as ErbB, PI3K-Akt, HIF-1, and mTOR signaling, and pathways  
86 that are related to innate immune responses such as TNF, NOD-like receptor (NLR) and RIG-I  
87 signaling (Fig. 1e). In addition, we observed upregulated platelet activation, complement  
88 cascades, FOXO signaling, and glycolysis (Fig. 1e), indicating that the SARS-CoV-2 infection  
89 induce pathways linked to thrombosis and metabolism.

90 To further capture the patterns of expression changes in response to the SARS-CoV-2 infection,  
91 we performed a weighted co-expression network analysis on both transcriptomic and proteomic  
92 datasets using all genes and proteins detected, their functional assignments, and the top genes  
93 (Fig. 1f) and proteins (Fig. 1g) in key network elements. For transcriptomic and proteomic  
94 networks (adjusted p value <0.01, Spearman  $\rho$  > 0.83), we identified a set of five transcriptomics  
95 and four proteomics communities of strongly interconnected genes and proteins (Fig. 1h). These  
96 communities were also validated against random networks. Characterization of these  
97 communities again highlighted several pathways of interest including HIF-1, mTOR, and TNF  
98 signaling previously observed in our pairwise comparisons and time series analyses (Fig 1e).  
99 Ranking of all communities based on their centrality further identified those that display a higher  
100 number of central genes/proteins, i.e. communities that exhibit a larger number of associated  
101 genes/proteins and thus capture most coordinated expression changes and hence are predicted to  
102 robustly influence network behavior. The two most central communities (Fig. 1f and 1g) entail  
103 several genes associated with AKT1, SLC2A1 (HIF-1 signaling), RAF1 (MAPK signaling),  
104 SEC13 (mTOR signaling) and Caspase 8 (CASP8; TNF signaling). Functional enrichment  
105 analysis indicated that these two communities were associated (adjusted  $p < 0.05$ ) with mTOR  
106 and MAPK signaling, Lysosomal and Proteasome-related processes, and cell cycle control.  
107 Importantly, we found that MAPK, AKT1, and mTOR showed cumulative expression changes  
108 through time (Fig. S1a and S2a); moreover, they were co-expressed (adjusted  $p < 0.05$ ) with  
109 several other genes/proteins, including those most central in each community (Fig. S1b,c and  
110 S2b,c), further highlighting the importance of these genes/proteins in coordinating the global  
111 response to infection. Finally, we found significant (adjusted  $p < 0.05$ ) functional overlap between  
112 three transcriptomic and three proteomic communities (communities 2, 3, 4; and communities A,  
113 B, D; Fig. 1h), thus pointing to common biological responses at the proteo-transcriptomic levels.  
114 These intersections included mTOR signaling (community 3 vs B), oxidative phosphorylation  
115 (communities 2,4 vs B) and thermogenesis (community 2,3,4 vs B), which are simultaneously

116 found among similar communities in transcriptomic and proteomic networks. Our functional and  
117 network community analyses identify common host cell genes (AKT1, MAPK) and biological  
118 pathways (mTOR, MAPK and HIF-1 signaling) that are upregulated in SARS-CoV-2 infected  
119 HuH7 cells.

120 **Dysregulated proteins and effector molecules in mTOR/HIF-1 signaling.** The top four  
121 identified pathways, ErbB, PI3K-Akt, HIF-1, and mTOR signaling showed overlap of several  
122 proteins like AKT1, mTOR, MAPK, 4E-BP1, and S6K as represented in Sankey plot (Fig 2a).  
123 Since all the top identified pathways converge at mTOR signaling, we wanted to investigate  
124 whether SARS-CoV-2 infections indeed change expression of critical effector molecules of the  
125 mTOR/HIF-1 signaling pathway, namely 4E-BP1, S6K1 and HIF-1 $\alpha$ . The mTOR pathway is  
126 involved in various biological functions and several viruses hijack this pathway to promote their  
127 own replication in different ways<sup>5</sup>. To this end the phosphorylation status of the effector  
128 molecules of the mTOR signaling was assessed during SARS-CoV-2 infection. The infection  
129 dynamics measured by SARS-CoV-2 RNA in the cell culture supernatant and in the cell is shown  
130 in Fig 2b. Western blot results showed that the phosphorylation states of 4E-BP1 and S6K1  
131 markedly changed during the course of the infection as compared to the mock infected control  
132 cells, showing a significant dip at 72 hpi (Fig 2c and 2d). Furthermore, HIF-1 $\alpha$  protein levels  
133 were rapidly reduced following SARS-CoV-2 infections (Fig 2c and 2d).

134 **Drug repurpose and viral host protein interactions of the dysregulated proteins.** To  
135 repurpose antiviral drugs targeting host-viral interactions is an attractive strategy to find drugs  
136 that might work against COVID-19. Therefore, we assessed protein-protein interactions including  
137 both host protein and SARS-CoV-2 protein associations obtained from the Human Protein Atlas  
138 (<https://www.proteinatlas.org/humanproteome/sars-cov-2>).<sup>6</sup> Proteins that were significantly  
139 increased between 24h and 48h after SARS-CoV-2 infection (Fig 2e) were arbitrarily assigned to  
140 early responses. A total of 108 host-viral protein interactions were observed. The majority of the  
141 interactions was observed with the viral protein M (13 interactions), followed by orf8 (12  
142 interactions), orf9c (11 interactions), nsp7, nsp8 (9 interactions) and nsp12 (8 interactions).  
143 Interestingly, while mapping these proteins with the pathway we observed that three HIF-1  
144 pathway-associated proteins were markedly altered in the infected cells: Heme Oxygenase 1  
145 (HMOX1), which interacts with orf3a, decreased over time, whereas Cullin 2 (CUL2) and Ring-  
146 Box 1 (RBX1), both of which interact with orf10, increased over time. In addition, we found that

147 the two Ras-associated proteins RAB8A and RAB2A interact with nsp7. Furthermore, we found  
148 that Receptor-interacting serine/threonine-protein kinase 1 (*RIPK1*), involved in NF- $\kappa$ B, NLR,  
149 RIG-I-like receptor and TNF signaling,<sup>7</sup> interacted with nsp12 and was significantly enriched  
150 over time (Fig 2e). Our data indicate a role of mTOR/HIF-1 in the cellular response to the SARS-  
151 CoV-2 infection, suggesting that drugs blocking this pathway could be possibly repurposed for  
152 COVID-19 patients (Fig 2f).

153  
154 **Discussion:**  
155 In this study using the integrated proteo-transcriptomics studies we identified four pathways,  
156 ErbB, HIF-1, mTOR and TNF signaling, among others that were markedly modulated during the  
157 course of the SARS-CoV-2 infection *in vitro*. Western blot validation of the downstream effector  
158 molecules of these pathways revealed a significant reduction in activated S6K1 and 4E-BP1 at 72  
159 hours post infection. The data therefore points towards dysregulation of mTOR/HIF-1 signaling  
160 cascades, which could be potential target for COVID-19 therapeutic interventions.

161  
162 The mTOR signaling pathways are known to regulate apoptosis, cell survival, and host  
163 transcription and translation and can be hijacked by several RNA viruses like influenza virus and  
164 coronaviruses.<sup>8-11</sup> PI3K activation results in AKT phosphorylation and subsequent activation of  
165 mTOR. Through a cascade of events, mTORC1 and AKT activates 4E-BP1 and eIF4 complex  
166 followed by translation of effector protein HIF-1 $\alpha$  that initiates host transcription and translation  
167 of specific genes. Another pathway that changed over time was the TNF signaling pathway. TNF  
168 signaling is also interlinked with HIF-1 signaling and can induce HIF-1 $\alpha$  through AKT and  
169 MAPK activation.<sup>12</sup> Of note, specific proteins dysregulated in the TNF signaling pathway were  
170 caspase 8, caspase 10,<sup>13</sup> and CCAAT/enhancer-binding protein beta (CEBPB),<sup>14</sup> which are linked  
171 to interferon (IFN) signaling and NF- $\kappa$ B signaling pathways. Previous studies on coronaviruses  
172 suggest a critical role of the IFN response, in particular IFN- $\beta$ .<sup>15,16</sup> This is also reflected in our  
173 findings that SARS-CoV-2 infections result in significantly dysregulated RIG-I, NLR and NF- $\kappa$ B  
174 pathways, which needs further evaluation. All these pathways have been linked to the IFN  
175 response.

176 It has been shown that absence of HIF-1 $\alpha$  can promote replication of influenza A virus and severe  
177 inflammation mediated via promotion of autophagy.<sup>17</sup> There could be several mechanisms that

178 result in decreased phosphorylation of mTOR effectors such as the host response affecting the  
179 translation machinery in response to stress or viral proteins at the late stage of infection that  
180 promote the translation of viral mRNAs by shutting down host mRNA translation. Nonetheless,  
181 similar to other viruses that hijacking the AKT/mTOR pathway such as the highly pathogenic  
182 1918 influenza virus<sup>8</sup> and the Middle East respiratory syndrome coronavirus (MERS-CoV),<sup>11</sup>  
183 deregulation of the mTOR pathway might enable SARS-CoV-2 to enhance its pathogenicity

184 A recent drug target network analysis based on potential human coronavirus and host interactions  
185 predicted that sirolimus (also known as rapamycin), which targets mTOR, could be repurposed.<sup>18</sup>  
186 Sirolimus was shown to inhibit MERS-CoV infection by 60% in mice.<sup>11</sup> Some studies have  
187 shown that everolimus, another mTOR inhibitor, and sirolimus are weakly active against  
188 influenza A virus.<sup>19,20</sup> Everolimus delayed death but was not able to reduce mortality in lethal  
189 mouse infection model of influenza A (H1N1 and H5N1).<sup>19</sup> Sirolimus was even shown to  
190 negatively affect the lung pathology probably due to its immunosuppressive effect.<sup>20</sup> It has also  
191 been reported to block viral protein expression and virion release, improving the prognosis in  
192 patients with severe H1N1 pneumonia and acute respiratory failure.<sup>21</sup> On the other hand,  
193 rapamycin treatment was shown to degrade antiviral barriers and could thus be potentially  
194 harmful in pathogenic viral infections.<sup>22</sup> In COVID-19 patients the severity of the disease is  
195 associated with a cytokine storm with markedly increased expression of interleukin 6 (IL-6) in  
196 the serum of severe cases.<sup>23</sup> Interestingly, IL-6 can activate mTOR in a STAT3 dependent or  
197 independent manner.<sup>24</sup> Whether our proposed drugs can be indeed repurposed for COVID-19  
198 therapies now needs to be carefully tested in *in vitro* SARS-CoV-2 infection models and in *in*  
199 *vivo* COVID-19 disease models.

200 There are some limitations of our study. First, we only used the HuH7 cell line but the SARS-  
201 CoV-2 can be also cultured in Vero E6, Vero CCL81, or HEK-293T cells. Whereas SARS-CoV-  
202 2 exerts rapid cytopathic effects in Vero E6 cells (within 24hpi), viral replication is slower in  
203 HuH7 and HEK293T cells, allowing to study host-cellular responses for 3 days after viral  
204 challenge<sup>25</sup>. Moreover, an earlier study used HuH7 cells to identify the transcriptomics signature  
205 of early cellular responses to SARS-CoV and HCoV-229E infections<sup>26</sup>. However, the observed  
206 effects could be cell type-specific and thus, we are currently assessing the effect of SARS-CoV-2  
207 infection in other cells lines. Moreover, SARS-CoV-2 has a propensity to mutate and our

208 experiments were performed with only one virus strain isolated from a Swedish patient. Of note,  
209 our virus isolate has close sequence similarity to the initial strains circulating in Wuhan, China.

210 In conclusions, we observed marked alterations of mTOR/HIF-1 signaling at the proteo-  
211 transcriptomic levels in response to SARS-CoV-2 infections, though the exact mechanistic role of  
212 these changes remains to be elucidated. Targeting mTOR/HIF-1 signaling could be an attractive  
213 candidate as a potential therapy, alone or preferably combined with antivirals, for the  
214 management of COVID-19 patients. Moreover, mTOR inhibition could be used to reduce the  
215 cytokine storm syndrome in severe cases of COVID-19.

216

## 217 **Methods**

218 **Cells and viruses.** The SARS-CoV-2 virus was isolated from a nasopharyngeal sample of a  
219 patient in Sweden and the isolated virus was confirmed as SARS-CoV-2 by sequencing (Genbank  
220 accession number MT093571). The hepatocyte derived cellular carcinoma cell line Huh7 was  
221 used. The cells were obtained from Marburg Virology Lab, Philipps-  
222 Universität Marburg, Marburg, Germany fully matching the STR reference profile of HuH-7.<sup>27</sup>

223 **SARS-CoV-2 infection of Huh7 cells.** Huh7 cells were plated in 6 well plates ( $2.5 \times 10^5$  cells/well)  
224 in DMEM (Thermo Fisher Scientific, US) supplemented with 10% heat-inactivated FBS (Thermo  
225 Fisher, US). At 90-95% cell confluence the medium was removed, cells washed carefully with  
226 PBS and thereafter either cultured in medium only (uninfected control) or infected with SARS-  
227 CoV-2 at a multiplicity of infection (MOI) of 1 added in a total volume of 0.5 mL. After 1 hr of  
228 incubation ( $37^\circ\text{C}$ , 5% $\text{CO}_2$ ) the inoculum was removed, cells washed with PBS and 2 mL DMEM  
229 supplemented with 5% heat-inactivated FBS was added to each well. Samples were collected at  
230 three different time points, 24, 48 and 72 hrs post-infection (hpi). Samples were collected for  
231 proteomics and western blot, and RNAseq.

232 **Total RNA extraction and Quantification of viral RNA.** The cells (uninfected, 24hpi, 48hpi and  
233 72hpi) were collected by adding Trizol™ (Thermo Fisher Scientific, US) directly to the wells.  
234 RNA from SARS-CoV-2 infected and uninfected Huh7 cells and supernatant was extracted using  
235 the Direct-zol RNA Miniprep (Zymo Research, US) and quantitative real-time polymerase chain  
236 reaction (qRT-PCR) was conducted using TaqMan Fast Virus 1-Step Master Mix (ThermoFisher  
237 Scientific, US) with primers and probe specific for the SARS-CoV-2 E gene following guidelines



238 by the World Health Organization ([https://www.who.int/docs/default-source/coronaviruse/wuhan-](https://www.who.int/docs/default-source/coronaviruse/wuhan-virus-assayv1991527e5122341d99287a1b17c111902.pdf)  
239 [virus-assayv1991527e5122341d99287a1b17c111902.pdf](https://www.who.int/docs/default-source/coronaviruse/wuhan-virus-assayv1991527e5122341d99287a1b17c111902.pdf)) as described previously <sup>4</sup>.

240 **Transcriptomics analysis (Illumina RNAseq).** The samples were sequenced using Illumina  
241 NextSeq550 in single-end mode with read length of 75 bases. The raw sequence data were first  
242 subjected to quality check using FastQC tool kit version 0.11.8. Illumina adapter sequences and  
243 low-quality bases were removed from the raw reads using the tool Trim Galore version 0.6.1.  
244 Phred score of 30 was used as cut-off to remove low quality bases. Quality of the data was again  
245 checked after pre-processing to assure high quality data for further analysis. The pre-processed  
246 reads were then aligned against human reference genome version 38 Ensembl release 96. Short  
247 read aligner STAR version 2.7.3a was used for the alignment. STAR was executed by setting the  
248 parameter soloStrand to Reverse to perform strand specific alignment and rest of the required  
249 parameters were set to default. The alignment result was written in sorted by co-ordinate bam  
250 format. After the alignment gene level read count data was generated for each sample using the  
251 module featureCounts from the software subread version 2.0.0. Read counting was performed by  
252 setting attribute type in the annotation to gene\_id and strand specificity to reverse. Human  
253 reference gene annotation version 38 Ensembl release 96 in gtf format was used for the read  
254 counting. Normalization factors were calculated using the R package edgeR <sup>28</sup> from read counts  
255 matrix to scale the raw library sizes. Low expression genes with maximum counts per million  
256 (CPM) values under 1 per sample were removed from the sample. As recommended in RNAseq,  
257 data were transformed to CPM and variance weight was calculated using voom function. Square  
258 root of residual standard deviation against log<sub>2</sub> CPMs was plotted to verify transformation  
259 quality.

260 **Protein extraction and in-solution digestion.** The cells (uninfected, 24hpi, 48hpi and 72hpi)  
261 were lysed in lysis buffer (5% glycerol, 10 mM Tris, 150 mM NaCl, 10% SDS and protease  
262 inhibitor), NuPAGE™ LDS sample buffer (ThermoFisher Scientific,US) was added and the  
263 samples was boiled at 99°C for 10 min. Aliquots of cell lysates (150 µL) were transferred to  
264 sample tubes and incubated at 37°C for 5 min at 550 rpm on a block heater and sonicated in  
265 water batch for 5 min. Each sample was reduced by adding 7 µL of 0.5M dithiothreitol (DTT) at  
266 37°C for 30 min and alkylated with 14 µL of 0.5M iodoacetamide for 30 min at room  
267 temperature (RT) in the dark. Following addition of 2 µL of concentrated phosphoric acid and  
268 1211 µL of binding buffer, protein capturing was performed according to the manufacturer's

269 protocol using S-Trap™ Micro spin columns (Protifi, Huntington, NY). After washing with 150  
270  $\mu\text{L}$  of binding buffer four times the samples were subjected to proteolytic digestion using 1.2  $\mu\text{g}$   
271 trypsin (sequencing grade, Promega) for 2h at 47°C. Then 40  $\mu\text{L}$  of 50 mM TEAB was added  
272 following acidification with 40  $\mu\text{L}$  of 0.2% formic acid (FA) and elution with 40  $\mu\text{L}$  of 50%  
273 acetonitrile (AcN)/0.2% FA and the eluents were dried using a Vacufuge vacuum concentrator  
274 (Eppendorf, US). The resulted peptides were cleaned up in a HyperSep filter plate with bed  
275 volume of 40  $\mu\text{L}$  (Thermo Fisher Scientific, Rockford, IL). Briefly, the plate was washed with  
276 80% AcN/0.1% FA and equilibrated with 0.1% FA. Samples were filtered in the plate and  
277 washed with 0.1% FA. Peptides were eluted with 30% AcN/0.1% FA and 80% AcN/0.1% FA  
278 and dried in a vacuum concentrator prior to tandem mass tag (TMT) labeling.

279 **TMT-Pro labeling.** Dry samples were dissolved in 30  $\mu\text{L}$  of 100 mM triethylammonium-  
280 bicarbonate (TEAB), pH 8, and 100  $\mu\text{g}$  of TMT-Pro reagents (Thermo Scientific,US) in 15  $\mu\text{L}$  of  
281 dry acetonitrile (AcN) were added. Samples were scrambled and incubated at RT at 550 rpm for  
282 2 h. The labeling reaction was stopped by adding 5  $\mu\text{L}$  of 5% hydroxylamine and incubated at RT  
283 with 550 rpm for 15 min. Individual samples were combined to one analytical sample and dried  
284 in vacuum concentrator.

285 **High pH reversed phase LC fractionation and RPLC-MS/MS analysis:** The TMTPro-labeled  
286 tryptic peptides were dissolved in 90  $\mu\text{L}$  of 20 mM ammonium hydroxide and were separated on  
287 an XBridge Peptide BEH C18 column (2.1  $\times$  mm inner diameter  $\times$  250  $\times$  mm, 3.5  $\mu\text{m}$  particle  
288 size, 300 Å pore size, Waters, Ireland) previously equilibrated with buffer A (20 mM  $\text{NH}_4\text{OH}$ )  
289 using a linear gradient of 1–23.5% buffer B (20  $\times$  mM  $\text{NH}_4\text{OH}$  in AcN, pH 10.0) in 42 min,  
290 23.5%-54% B in 4 min and 54-63% B in 2  $\times$  min at a flow rate of 200  $\times$   $\mu\text{L}/\text{min}$ . The  
291 chromatographic performance was monitored by sampling eluate with a UV detector (Ultimate  
292 3000 UPLC, Thermo Scientific, US) monitoring at 214  $\times$  nm. Fractions were collected at 30 s  
293 intervals into a 96-well plate and combined into 12 samples concatenating eight fractions  
294 representing the peak peptide elution. Each combined fraction sample (800  $\mu\text{L}$ ) was dried in a  
295 vacuum concentrator and the peptides was resuspended in 2% AcN/0.1% FA prior to LC-MS/MS  
296 analysis.

297 Approximately, 2 $\mu\text{g}$  samples were injected in an Ultimate 3000 nano LC on-line coupled to an  
298 Orbitrap Fusion Lumos mass spectrometer (Thermo Scientific, San José, CA). The

299 chromatographic separation of the peptides was achieved using a 50 cm long C18 Easy spray  
300 column (Thermo Scientific,US) at 55°C, with the following gradient: 4-26% of solvent B (2%  
301 AcN/0.1% FA) in 120 min, 26-95% in 5 min, and 95% of solvent B for 5 min at a flow rate of  
302 300 nL/min. The MS acquisition method was comprised of one survey full mass spectrum  
303 ranging from  $m/z$  350 to 1700, acquired with a resolution of  $R=120,000$  (at  $m/z$  200) targeting  
304  $4 \times 10^5$  ions and 50 ms maximum injection time (max IT), followed by data-dependent HCD  
305 fragmentations of precursor ions with a charge state 2+ to 7+ for 2 s, using 60 s dynamic  
306 exclusion. The tandem mass spectra were acquired with a resolution of  $R=50,000$ , targeting  
307  $5 \times 10^4$  ions and 86 ms max IT, setting isolation width to  $m/z$  1.4 and normalized collision energy  
308 to 35% setting first mass at  $m/z$  100.

309 **Peptide identification and preprocessing.** The raw files were imported to Proteome Discoverer  
310 v2.4 (Thermo Scientific) and searched against the *Homo sapiens* SwissProt (2020\_01 release  
311 with 20,595 entries) and the pre-leased SARS-CoV-2 UniProt (completed with 14 SARS-CoV2  
312 sequences of COVID-19 UniProtKB release 2020\_04\_06) protein databases with Mascot v 2.5.1  
313 search engine (MatrixScience Ltd., UK). Parameters were chosen to allow two missed cleavage  
314 sites for trypsin while the mass tolerance of precursor and HCD fragment ions was 10 ppm and  
315 0.05 Da, respectively. Carbamidomethylation of cysteine (+57.021 Da) was specified as a fixed  
316 modification, whereas TMTPro at peptide N-terminus and lysine, oxidation of methionine  
317 (+15.995 Da), deamidation of asparagine and glutamine were defined as variable modifications.  
318 For quantification both unique and razor peptides were requested. Protein raw data abundance  
319 was first filtered for empty rows with *in house* script and quantile-normalize using R package  
320 NormalyzerDE<sup>29</sup>. Principal component analysis (PCA) was applied to explore sample-to- sample  
321 relationships. One proteomics samples from the uninfected control was excluded as it turned out  
322 to be outlier.

323 **Statistical analysis.** Proteomics and transformed transcriptomics data were tested for normality  
324 using histograms with normal distribution superimposed. Differential expression through linear  
325 model was performed using R package LIMMA<sup>30</sup>. LIMMA supports multifactor designed  
326 experiments in microarray, transcriptomics and proteomics. Its features are designed to support  
327 small number of arrays. The three infected replicates at 24hpi, 48hpi and 72hpi hours  
328 respectively were selected in order to perform an equi-spaced univariate time series analysis. In  
329 limma design matrix, separated coefficients were associated with time and replicates in order to

330 extract the difference as a contrast. Moderated paired-t-test using limma with adjustment for  
331 replicates was applied. For pairwise comparisons, single factorial design was implemented to fit  
332 model with a coefficient for each of our four factors: uninfected, 24hpi, 48hpi and 72hpi.  
333 Comparisons were extracted as contrasts. In both analysis, significant differential genes and  
334 proteins were selected based on p values after Benjamini-Hochberg (BH) adjustment. Genes with  
335 alpha value inferior to 0.05 were considered significant.

336 **Bioinformatics Analysis:** The transcriptomics and proteomics analysis were performed using all  
337 the protein coding genes and proteins and a gene set of viral processes, response and diseases  
338 respectively. The viral response gene set is a catalogue of genes which are known to have involve  
339 in viral processes, response and diseases. The catalogue was enriched by mining biological  
340 process category of gene-ontology terms, Reactome pathways and gene sets associated with  
341 various viral diseases. Gene Ontology terms were selected by keeping, “response to virus  
342 (GO:0009615)” as parent term. All child terms of GO:0009615 were selected based on ontology  
343 term relationship “is a” and “regulates”. The pathway “Antiviral mechanism by IFN-stimulated  
344 genes” and two other events it participates were selected from Reactome database. Gene sets  
345 related to 42 virus associated diseases and six virus related diseases were selected  
346 from “Rare\_Diseases\_AutoRIF\_Gene\_Lists” library provided by gene set enrichment  
347 tool Enrichr<sup>31</sup>. The viral response gene set contains total of 1517 protein coding genes. After  
348 filtering antiviral genes, up and downregulated proteins and transcripts were submitted separately  
349 to gene set enrichment analysis (GSEA) using gseapy v0.9.17.

350 R package gplots v3.03 was used to generate heatmaps to display terms associated adjusted p  
351 values contrasts over conditions.

352 **Network and community analyses.** Association analyses were performed by computing  
353 pairwise Spearman rank correlations for all features after removing null variant or genes with  
354 very low expression (RPKM < 1). Correlations were considered statistically significant at FDR <  
355 0.01. Positive correlations were selected and used to build a weighted graph where Spearman  $\rho$   
356 was used as weights. All network analyses were performed in igraph<sup>32</sup>. For all networks,  
357 diameter, average path lengths, clustering coefficients, and degree distributions were compared  
358 with those attained for similarly-sized random networks (Erdős-Rényi models,<sup>33</sup>). Degree  
359 centrality was computed for all networks and normalized for network size. Communities were

360 identified by modularity maximization through the Leiden algorithm<sup>34</sup>. Community centrality  
361 was computed by averaging node centrality and used to identify the most central communities in  
362 each network by degree comparison. Gene set enrichment analysis was performed on each  
363 community ( $n > 30$ ) through Enrichr for KEGG Human 2019 where backgrounds were selected  
364 based on the node number of each network. Community similarity was computed through  
365 hypergeometric testing of overlap between statistically significant KEGG terms for each  
366 transcriptomic vs proteomic pair of communities. Throughout, all statistical tests were considered  
367 at an FDR  $< 0.05$  unless otherwise stated. All analyses were performed in Python 3.7.

368 Protein-protein interactions among human proteins were derived from Human Reference  
369 Interactome (HuRI). Interactions between human proteins and SARS-Cov2 viral proteins were  
370 obtained from Human Protein Atlas (HPA). Protein interaction network is created using  
371 Cytoscape version 3.6.1<sup>35</sup>. Edge weighted spring embedded layout was used for the network. R  
372 package gplots 3.03 was used to generate heatmaps to display terms associated p values contrasts  
373 over conditions. Sankey Plot illustrates most important contribution genes to flow pathways. It  
374 was plotted using R package ggalluvial version 0.11.1<sup>36</sup>. Scatter plots produced using ggplot2  
375 represent the bivariate relationship between proteins and time.

376 **Western Blot.** Evaluation of protein expression was performed by running 20  $\mu$ g of total protein  
377 lysate on NuPage Bis Tris 4-12%, gels or NuPage Tris-Acetate 3-8% gels (Invitrogen, Carlsbad,  
378 CA, USA). Proteins were transferred using iBlot dry transfer system (Invitrogen, Carlsbad, CA,  
379 USA) and blocked for 1h using 5% milk or bovine serum albumin (BSA) in 0.1% PBSt (0.1%  
380 Tween-20). Subsequent antibody detection was performed at 4°C over-night or 2h at room  
381 temperature for  $\beta$ -Actin. Membranes were washed using 0.1% PBSt and secondary antibody  
382 incubated 1h at room-temperature using Dako Polyconal Goat Anti-Rabbit or Anti-Mouse  
383 Immunoglobulins/HRP (Aglient Technologies, Santa Clara, CA, USA) washed using 0.1% PBSt  
384 and visualized using ECL or ECL Select (GE Healthcare, Chicago, IL, USA) on ChemiDoc  
385 XRS+ System (Bio-Rad Laboratories, Hercules, CA, USA). The western blot analysis was  
386 performed on duplicates (p-mTOR, S6K and p-S6K) or triplicate (4E-BP1, p-4E-BP1 and HIF-  
387 1 $\alpha$ ) of the samples in two different timepoints. Viral RNA was quantified from cells as well as  
388 supernatant in all the time points as a confirmation of the infection. The uncropped western blots  
389 are given as resource data file 1.

390 **Data and Code Availability.** The raw RNAseq data can be obtained from the SRA using the  
391 project id. PRJNA627100. Proteomics data can be obtained from  
392 <https://zenodo.org/record/3754719#.XqgnSy2B30Q>. All the codes are available at github:  
393 <https://github.com/neogilab/COVID19>

394 **Reference:**

- 395 1 Dong, E., Du, H. & Gardner, L. An interactive web-based dashboard to track COVID-19  
396 in real time. *Lancet Infect Dis*, doi:10.1016/s1473-3099(20)30120-1 (2020).
- 397 2 Zhou, P. *et al.* A pneumonia outbreak associated with a new coronavirus of probable bat  
398 origin. *Nature* **579**, 270-273, doi:10.1038/s41586-020-2012-7 (2020).
- 399 3 Wu, F. *et al.* A new coronavirus associated with human respiratory disease in China.  
400 *Nature* **579**, 265-269, doi:10.1038/s41586-020-2008-3 (2020).
- 401 4 Monteil, V. *et al.* Inhibition of SARS-CoV-2 infections in engineered human tissues using  
402 clinical-grade soluble human ACE2. *Cell* (2020).
- 403 5 Luo, Q. *et al.* mTORC1 Negatively Regulates the Replication of Classical Swine Fever  
404 Virus Through Autophagy and IRES-Dependent Translation. *iScience* **3**, 87-101,  
405 doi:10.1016/j.isci.2018.04.010 (2018).
- 406 6 Gordon, D. E. *et al.* A SARS-CoV-2-human protein-protein interaction map reveals drug  
407 targets and potential drug-repurposing. *BioRxiv* (2020).
- 408 7 Weinlich, R. & Green, D. R. The two faces of receptor interacting protein kinase-1. *Mol*  
409 *Cell* **56**, 469-480, doi:10.1016/j.molcel.2014.11.001 (2014).
- 410 8 Ranadheera, C., Coombs, K. M. & Kobasa, D. Comprehending a Killer: The Akt/mTOR  
411 Signaling Pathways Are Temporally High-Jacked by the Highly Pathogenic 1918  
412 Influenza Virus. *EBioMedicine* **32**, 142-163, doi:10.1016/j.ebiom.2018.05.027 (2018).
- 413 9 Ehrhardt, C. & Ludwig, S. A new player in a deadly game: influenza viruses and the  
414 PI3K/Akt signalling pathway. *Cell Microbiol* **11**, 863-871, doi:10.1111/j.1462-  
415 5822.2009.01309.x (2009).
- 416 10 Mizutani, T., Fukushi, S., Saijo, M., Kurane, I. & Morikawa, S. JNK and PI3k/Akt  
417 signaling pathways are required for establishing persistent SARS-CoV infection in Vero  
418 E6 cells. *Biochim Biophys Acta* **1741**, 4-10, doi:10.1016/j.bbadis.2005.04.004 (2005).
- 419 11 Kindrachuk, J. *et al.* Antiviral potential of ERK/MAPK and PI3K/AKT/mTOR signaling  
420 modulation for Middle East respiratory syndrome coronavirus infection as identified by

- 421 temporal kinome analysis. *Antimicrob Agents Chemother* **59**, 1088-1099,  
422 doi:10.1128/aac.03659-14 (2015).
- 423 12 Zhou, J., Callapina, M., Goodall, G. J. & Brune, B. Functional integrity of nuclear factor  
424 kappaB, phosphatidylinositol 3'-kinase, and mitogen-activated protein kinase signaling  
425 allows tumor necrosis factor alpha-evoked Bcl-2 expression to provoke internal ribosome  
426 entry site-dependent translation of hypoxia-inducible factor 1alpha. *Cancer Res* **64**, 9041-  
427 9048, doi:10.1158/0008-5472.can-04-1437 (2004).
- 428 13 Chen, H., Ning, X. & Jiang, Z. Caspases control antiviral innate immunity. *Cell Mol*  
429 *Immunol* **14**, 736-747, doi:10.1038/cmi.2017.44 (2017).
- 430 14 Zwergal, A. *et al.* C/EBP beta blocks p65 phosphorylation and thereby NF-kappa B-  
431 mediated transcription in TNF-tolerant cells. *J Immunol* **177**, 665-672,  
432 doi:10.4049/jimmunol.177.1.665 (2006).
- 433 15 Hensley, L. E. *et al.* Interferon-beta 1a and SARS coronavirus replication. *Emerg Infect*  
434 *Dis* **10**, 317-319, doi:10.3201/eid1002.030482 (2004).
- 435 16 Spiegel, M. *et al.* Inhibition of Beta interferon induction by severe acute respiratory  
436 syndrome coronavirus suggests a two-step model for activation of interferon regulatory  
437 factor 3. *J Virol* **79**, 2079-2086, doi:10.1128/jvi.79.4.2079-2086.2005 (2005).
- 438 17 Zhao, C. *et al.* Deficiency of HIF-1alpha enhances influenza A virus replication by  
439 promoting autophagy in alveolar type II epithelial cells. *Emerg Microbes Infect* **9**, 691-  
440 706, doi:10.1080/22221751.2020.1742585 (2020).
- 441 18 Zhou, Y. *et al.* Network-based drug repurposing for novel coronavirus 2019-  
442 nCoV/SARS-CoV-2. *Cell Discov* **6**, 14, doi:10.1038/s41421-020-0153-3 (2020).
- 443 19 Murray, J. L. *et al.* Inhibition of influenza A virus replication by antagonism of a PI3K-  
444 AKT-mTOR pathway member identified by gene-trap insertional mutagenesis. *Antivir*  
445 *Chem Chemother* **22**, 205-215, doi:10.3851/imp2080 (2012).
- 446 20 Alsuwaidi, A. R. *et al.* Sirolimus alters lung pathology and viral load following influenza  
447 A virus infection. *Respir Res* **18**, 136, doi:10.1186/s12931-017-0618-6 (2017).
- 448 21 Wang, C. H. *et al.* Adjuvant treatment with a mammalian target of rapamycin inhibitor,  
449 sirolimus, and steroids improves outcomes in patients with severe H1N1 pneumonia and  
450 acute respiratory failure. *Crit Care Med* **42**, 313-321,  
451 doi:10.1097/CCM.0b013e3182a2727d (2014).

- 452 22 Shi, G., Ozog, S., Torbett, B. E. & Compton, A. A. mTOR inhibitors lower an intrinsic  
453 barrier to virus infection mediated by IFITM3. *Proc Natl Acad Sci U S A* **115**, E10069-  
454 e10078, doi:10.1073/pnas.1811892115 (2018).
- 455 23 Zhao, M. Cytokine storm and immunomodulatory therapy in COVID-19: role of  
456 chloroquine and anti-IL-6 monoclonal antibodies. *Int J Antimicrob Agents*, 105982,  
457 doi:10.1016/j.ijantimicag.2020.105982 (2020).
- 458 24 Pinno, J. *et al.* Interleukin-6 influences stress-signalling by reducing the expression of the  
459 mTOR-inhibitor REDD1 in a STAT3-dependent manner. *Cell Signal* **28**, 907-916,  
460 doi:10.1016/j.cellsig.2016.04.004 (2016).
- 461 25 Harcourt, J. *et al.* Severe Acute Respiratory Syndrome Coronavirus 2 from Patient with  
462 2019 Novel Coronavirus Disease, United States. *Emerg Infect Dis* **26**,  
463 doi:10.3201/eid2606.200516 (2020).
- 464 26 Tang, B. S. *et al.* Comparative host gene transcription by microarray analysis early after  
465 infection of the Huh7 cell line by severe acute respiratory syndrome coronavirus and  
466 human coronavirus 229E. *J Virol* **79**, 6180-6193, doi:10.1128/jvi.79.10.6180-6193.2005  
467 (2005).
- 468 27 Rohde, C., Becker, S. & Kraehling, V. Marburg virus regulates the IRE1/XBP1-dependent  
469 unfolded protein response to ensure efficient viral replication. *Emerg Microbes Infect* **8**,  
470 1300-1313, doi:10.1080/22221751.2019.1659552 (2019).
- 471 28 Robinson, M. D., McCarthy, D. J. & Smyth, G. K. edgeR: a Bioconductor package for  
472 differential expression analysis of digital gene expression data. *Bioinformatics* **26**, 139-  
473 140, doi:10.1093/bioinformatics/btp616 (2010).
- 474 29 Willforss, J., Chawade, A. & Levander, F. NormalyzerDE: Online Tool for Improved  
475 Normalization of Omics Expression Data and High-Sensitivity Differential Expression  
476 Analysis. *J Proteome Res* **18**, 732-740, doi:10.1021/acs.jproteome.8b00523 (2019).
- 477 30 Ritchie, M. E. *et al.* limma powers differential expression analyses for RNA-sequencing  
478 and microarray studies. *Nucleic Acids Res* **43**, e47, doi:10.1093/nar/gkv007 (2015).
- 479 31 Kuleshov, M. V. *et al.* Enrichr: a comprehensive gene set enrichment analysis web server  
480 2016 update. *Nucleic Acids Res* **44**, W90-97, doi:10.1093/nar/gkw377 (2016).
- 481 32 Csardi, G. & Nepusz, T. The igraph software package for complex network research.  
482 *InterJournal, complex systems* **1695**, 1-9 (2006).



- 483 33 Erdős, P. & Rényi, A. On the strength of connectedness of a random graph. *Acta*  
484 *Mathematica Hungarica* **12**, 261-267 (1961).
- 485 34 Traag, V. A., Waltman, L. & van Eck, N. J. From Louvain to Leiden: guaranteeing well-  
486 connected communities. *Sci Rep* **9**, 5233, doi:10.1038/s41598-019-41695-z (2019).
- 487 35 Brysbaert, G., Mauri, T. & Lensink, M. F. Cytoscape [version 1; referees: 3 approved].  
488 (2018).
- 489 36 Riehm, P., Hanfler, M. & Froehlich, B. in *IEEE Symposium on Information*  
490 *Visualization, 2005. INFOVIS 2005*. 233-240 (IEEE).

491

492 **Acknowledgements:** The study is funded by the Swedish Research Council Grant (2017-01330,  
493 UN). A. M. is supported by the Swedish research Council 2018-05766 and 2017-03126. J.M.P. is  
494 supported by the Canada 150 Research Chair program and CIHR rapid Response COVID-19  
495 grant. We would like to thank the core facility Bioinformatics and Expression Analysis (BEA),  
496 supported by the board of research at the Karolinska Institute and the research committee at the  
497 Karolinska hospital specifically Fredrik Fagerström-Billai and Carolina Bonilla Karlsson for  
498 rapidly performing the RNAseq run. We also like to thank Proteomics Biomedicum; Karolinska  
499 Institute, Solna, and National Bioinformatics Infrastructure Support, Sweden for supporting the  
500 project. The computations were performed on resources provided by SNIC through Uppsala  
501 Multidisciplinary Center for Advanced Computational Science (UPPMAX) under Project  
502 SNIC2017-550 Authors also like to thank Beatriz Sá Vinhas and Elisa Saccon for continuous  
503 discussion and performing the literature review for the article.

504 **Authors Contributions:**

505 S.A. performed all the infection experiments, S.G., S.S.A., M.S. and S.K. performed the other lab  
506 experiments and wrote the method and result part of the manuscript, A.T.A., F.M., K.S. and R.B.  
507 performed the bioinformatics analysis and wrote the method and result part of the manuscript.  
508 Á.V. and M.S. performed the mass-spectrometry and wrote the method part of the manuscript,  
509 J.M.P. and A.M. contributed with resource and manuscript writing and revision. S.G. and U.N.  
510 wrote the first draft of the manuscript reviewed by J.M.P., A.M. U.N. conceived and designed the  
511 study and contributed with resource. All authors approved the final version of the manuscript.

512 **Figure Legends:**

513 **Figure 1. (a)** Brief methodology. **(b)** Viral RNA quantification using qPCR targeting the E gene  
514 of SARS-CoV-2. **(c)** Detected viral genes and open reading frame in the RNAseq experiment. **(d)**  
515 Temporal dynamics of detected proteins in the HuH7 cells by TMT-MS. **(e)** Gene set enrichment  
516 analysis using the genes related to viral response, process and diseases in single omics level by  
517 pairwise comparative analysis and time series analysis at individual omics level. Significant  
518 (adjusted p values) KEGG terms enriched for upregulated genes were represented as heatmap.  
519 The lower adjusted p values are shown in dark red color and higher ones with light red color,  
520 non-significant pathways are represented in grey color. **(f-g)** Network analysis using genes and  
521 proteins. Analysis of the most central communities in each network highlights key KEGG terms  
522 (right) among the top 10% associated genes and proteins. The top 10% correlations (Spearman  
523  $\rho > 0.95$ , FDR  $< 0.05$ ) were selected in the most central community in transcriptomic **(f)** and  
524 proteomic **(g)** networks (inset) based on mean normalized degree. The top KEGG terms  
525 associated with each of the two communities (FDR  $< 0.05$ ) are highlighted, as well as genes that  
526 had been previously found in Fig 1e. **(h).** A proteo-transcriptomic network analysis highlights  
527 coordinated expression and functional changes in response to viral infection. Communities  
528 (circles) in transcriptomic and proteomic networks, where node size is proportion to the number  
529 of elements (728 - 2519). Edges indicate association ( $Q < 0.05$ ) with KEGG terms (dashed),  
530 network edges (solid red and blue), or community similarity (solid gray).

531 **Figure 2. (a)** Top four pathways, ErbB signaling, HIF-1 signaling, mTOR signaling and TNF  
532 signaling were selected and, together with proteins that are altered in the infection course,  
533 represented as Sankey Plot in order to illustrate the most important contribution to the flow of  
534 each pathway. **(b)** HuH7 cells were infected with SARS-CoV-2 at MOI of 1 and cells were  
535 harvested at 24hpi, 48hpi and 72hpi. The viral RNA quantification using qPCR targeting the E  
536 gene of SARS-CoV-2 targeting the supernatant. The relative fold change with respect to the  
537 uninfected controls is shown. **(c)** The representative western blots of indicated antibodies with **(d)**  
538 densitometric quantification are shown. **(e)** Network visualizing protein interactions among  
539 significantly changing proteins between samples at 24hpi and 48hpi, and SARS-CoV-2 viral  
540 proteins. Green color nodes represent decreased proteins at 48hpi and red colored proteins  
541 represent increased proteins at 48hpi. Size of the nodes are relative to their log<sub>2</sub> fold change.  
542 Hexagonal shaped nodes denote SARS-CoV-2 viral proteins. The edges are derived from Human  
543 Reference Interactom (HuRI) and SARS-CoV-2 entry in Human Protein Atlas. **(f)** Approved

544 drugs targeting AKT/mTOR/HIF-1 signaling pathway. Only key proteins of the pathway are  
545 shown. The inhibitors are shown in red and activators in green.

546

547 **Supplementary Materials:**

548 **Figure S1** – Gene expression (A) and co-expression (B – C) among key genes and top correlated  
549 and central genes in each community identified based on a transcriptomic network (communities  
550 1-5). For each community we identified selected the top 10 genes (gray labels), ranked by their  
551 median centrality (median ranked degree, betweenness, closeness and eccentricity centralities),  
552 among the top 10% correlated gene in each community. Key proteins, previously associated with  
553 HIF-1a, mTOR, MAPK signaling and other top pathways, are highlighted in black (Fig. 1e).  
554 Spearman rank correlations were computed for all genes (B) and excluded if not statistically  
555 significant (C, FDR < 0.01). S6K-A3, S6K-B2, and 4E-BP1 respectively indicate genes  
556 RPS6KA3, RPS6KB2, and EIF4EBP1.

557

558 **Figure S2** – Protein abundance (A) and correlations (B – C) among key proteins and top  
559 correlated and central proteins in each community identified based on a proteomic network  
560 (communities A-D). For each community we identified selected the top 10 proteins (gray labels),  
561 ranked by their median centrality (median ranked degree, betweenness, closeness and eccentricity  
562 centralities), among the top 10% correlated proteins in each community. Key proteins, previously  
563 associated with HIF-1a, mTOR, MAPK signaling and other top pathways, are highlighted in  
564 black (Fig. 1e). Spearman rank correlations were computed for all proteins (B) and excluded if  
565 not statistically significant (C, FDR < 0.01). S6K-A3, S6K-B2, and 4E-BP1 respectively indicate  
566 genes RPS6KA3, RPS6KB2, and EIF4EBP1. Note that 4E-BP1 is among the top 10% most  
567 correlated genes in community B.

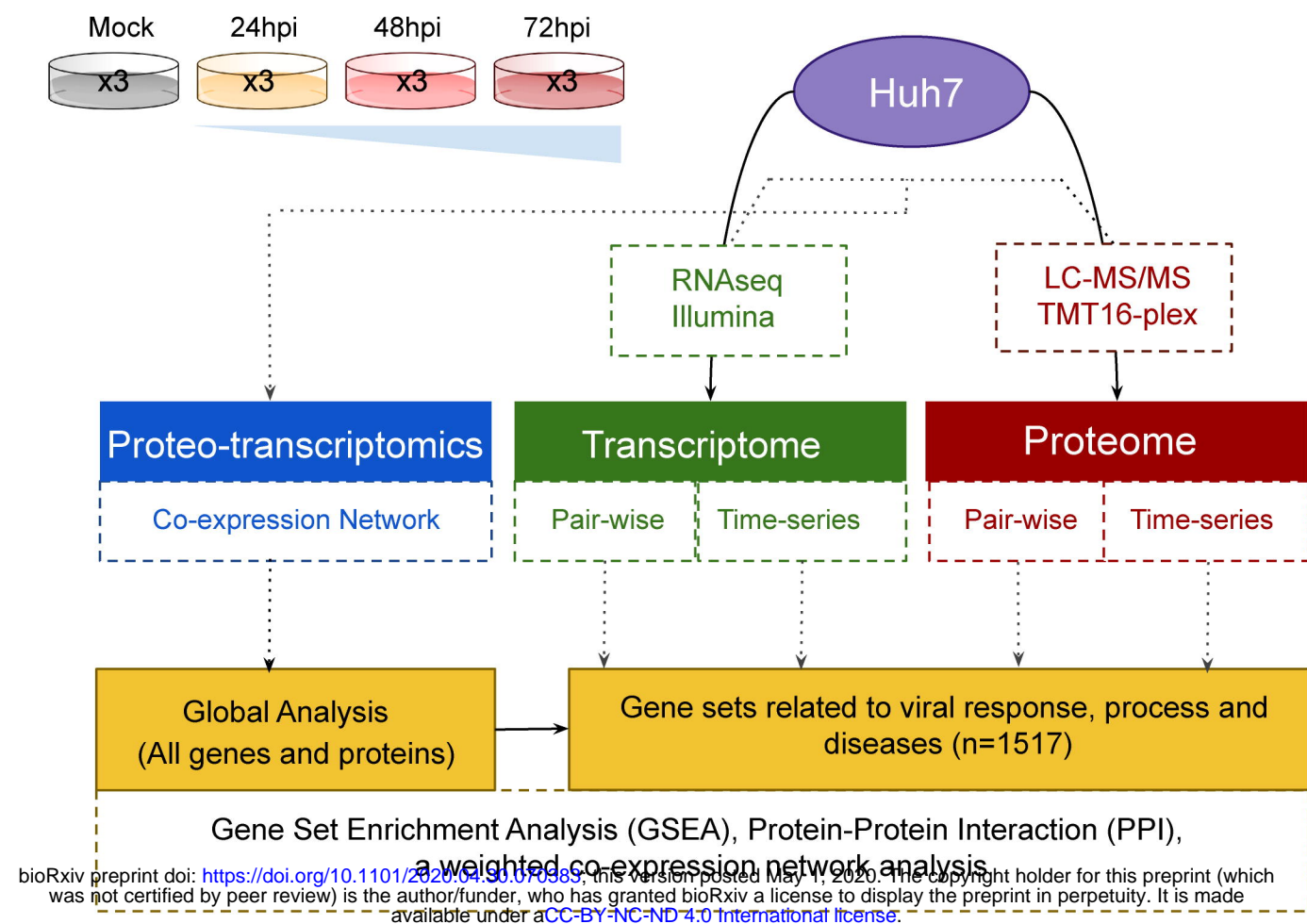
568

569 **Supplementary Source Data 1.** Original western blot.

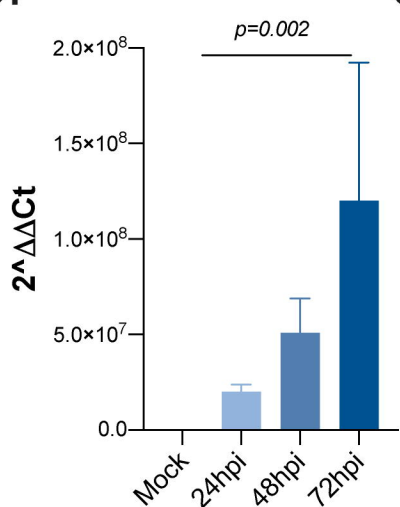
570

571

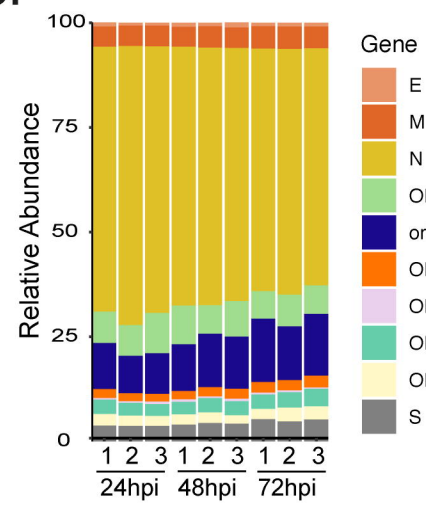
a.



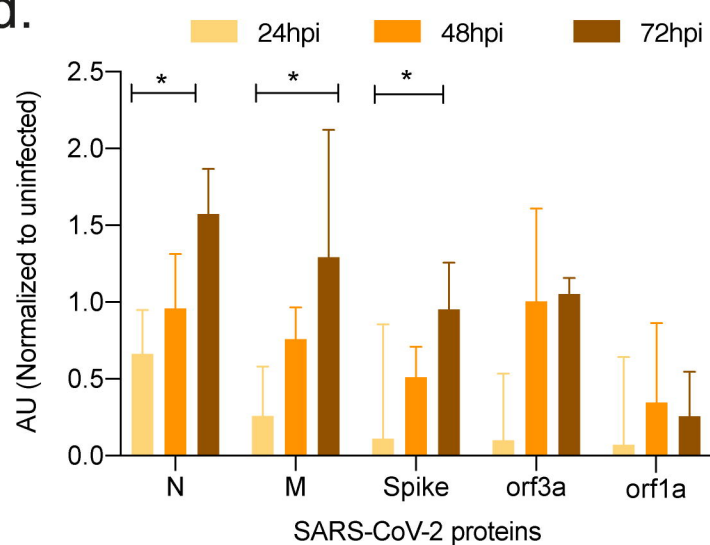
b.



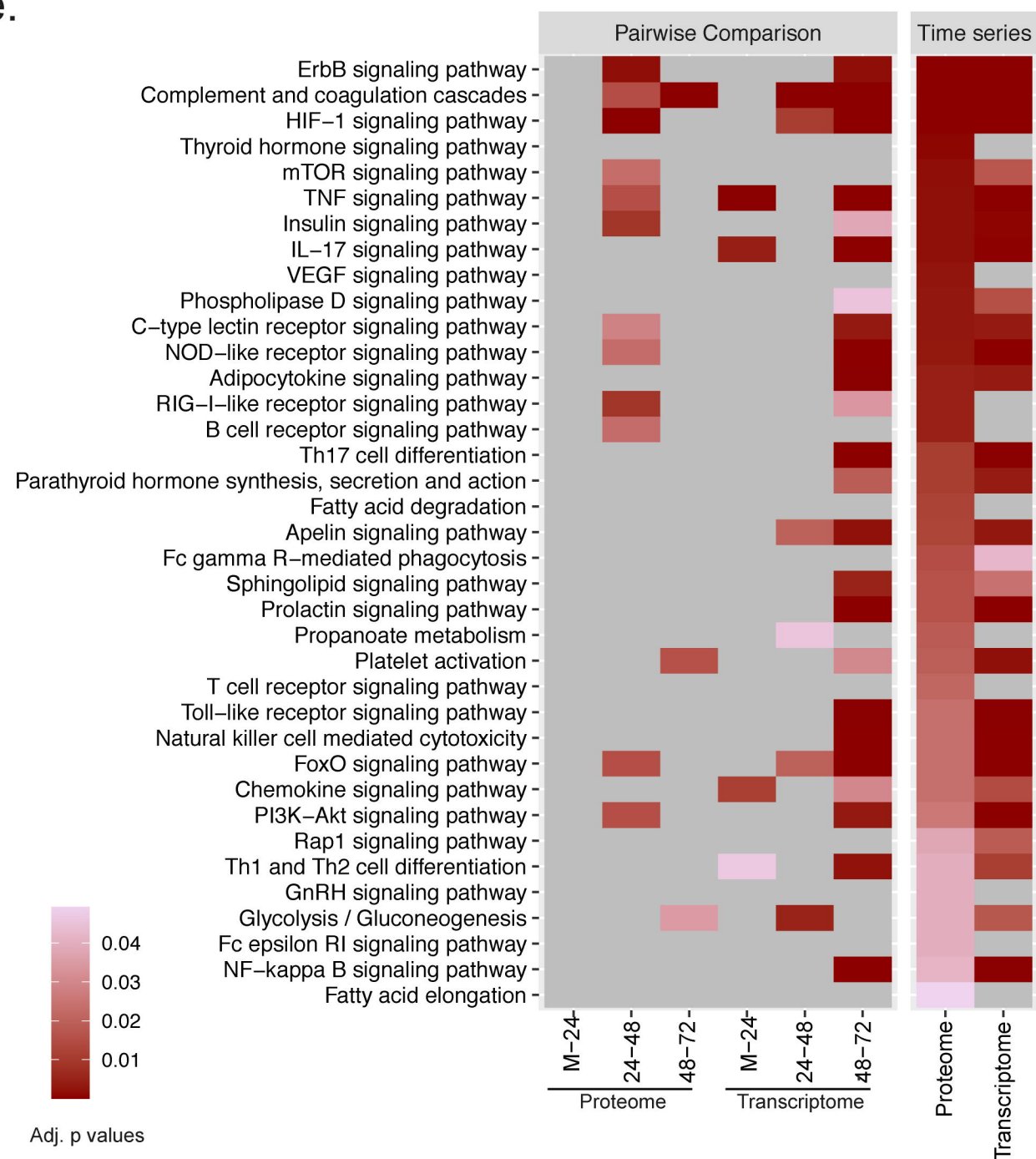
c.



d.

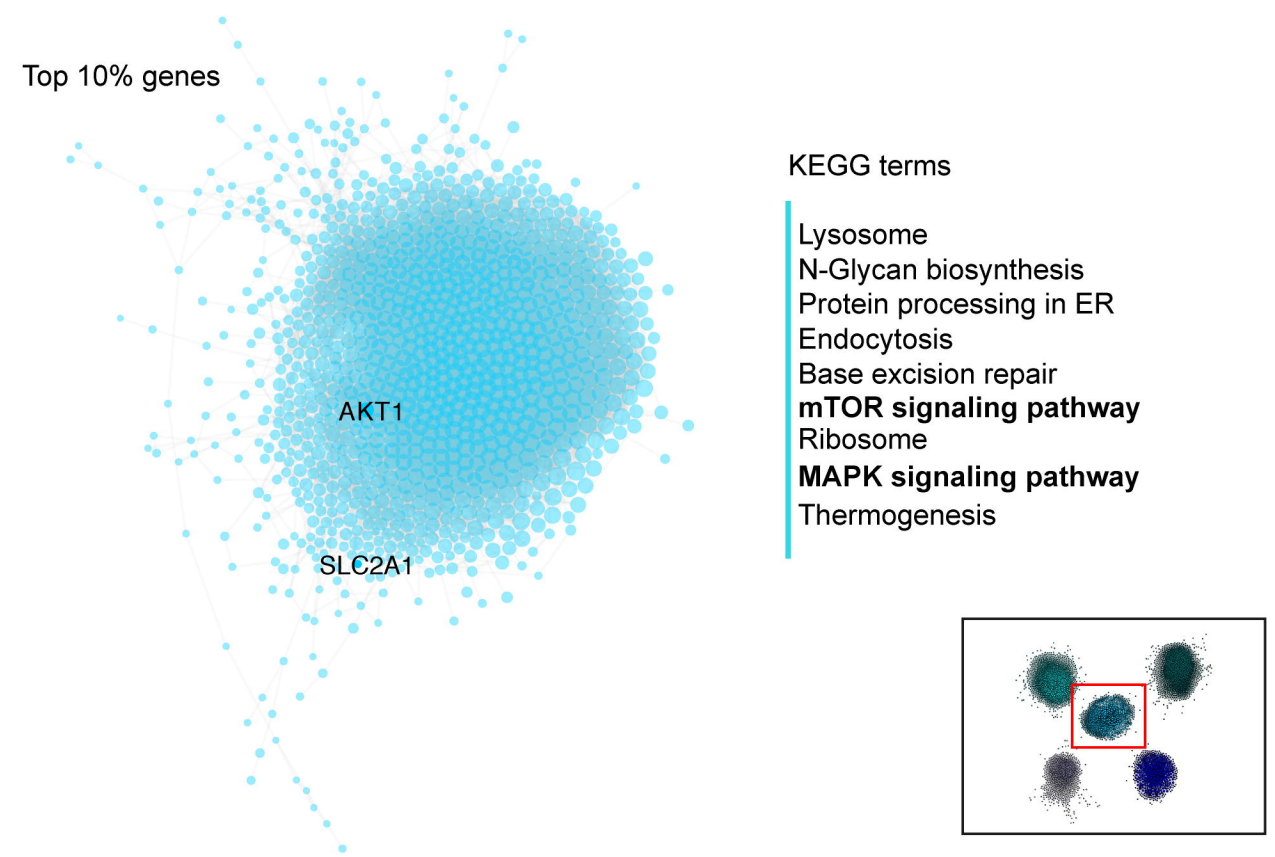


e.



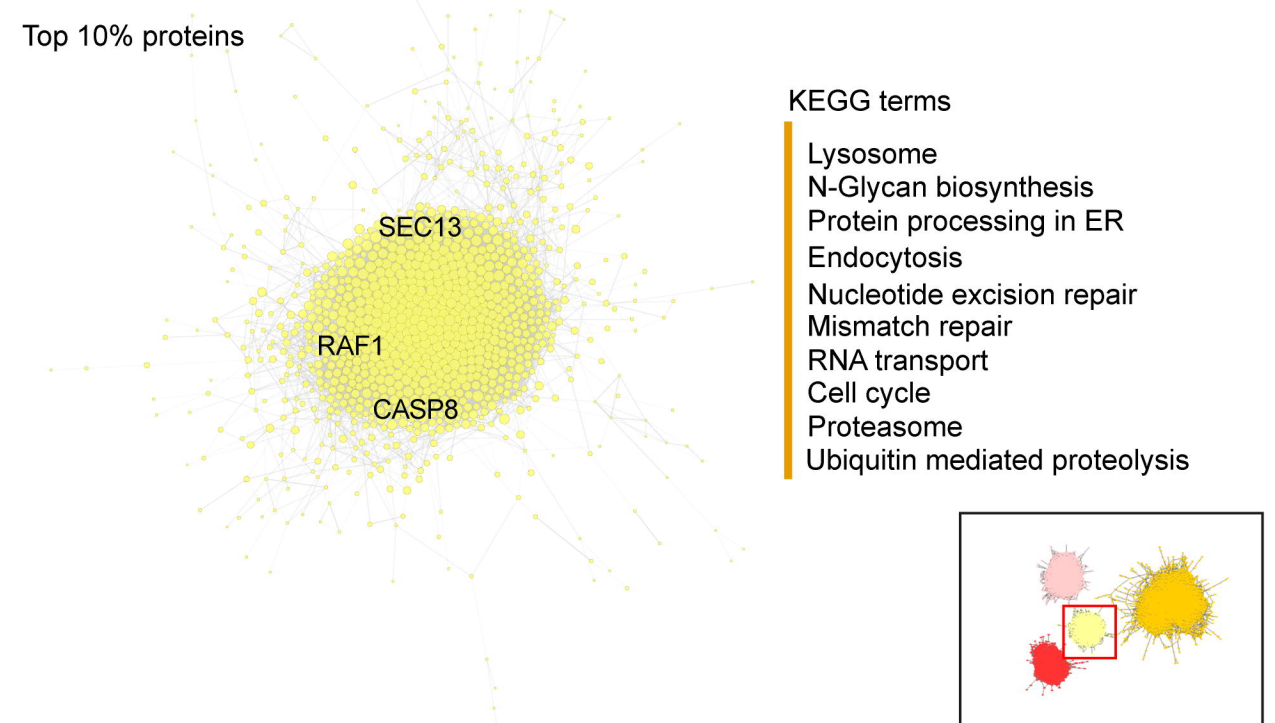
f.

Transcriptomic network (Community 3)

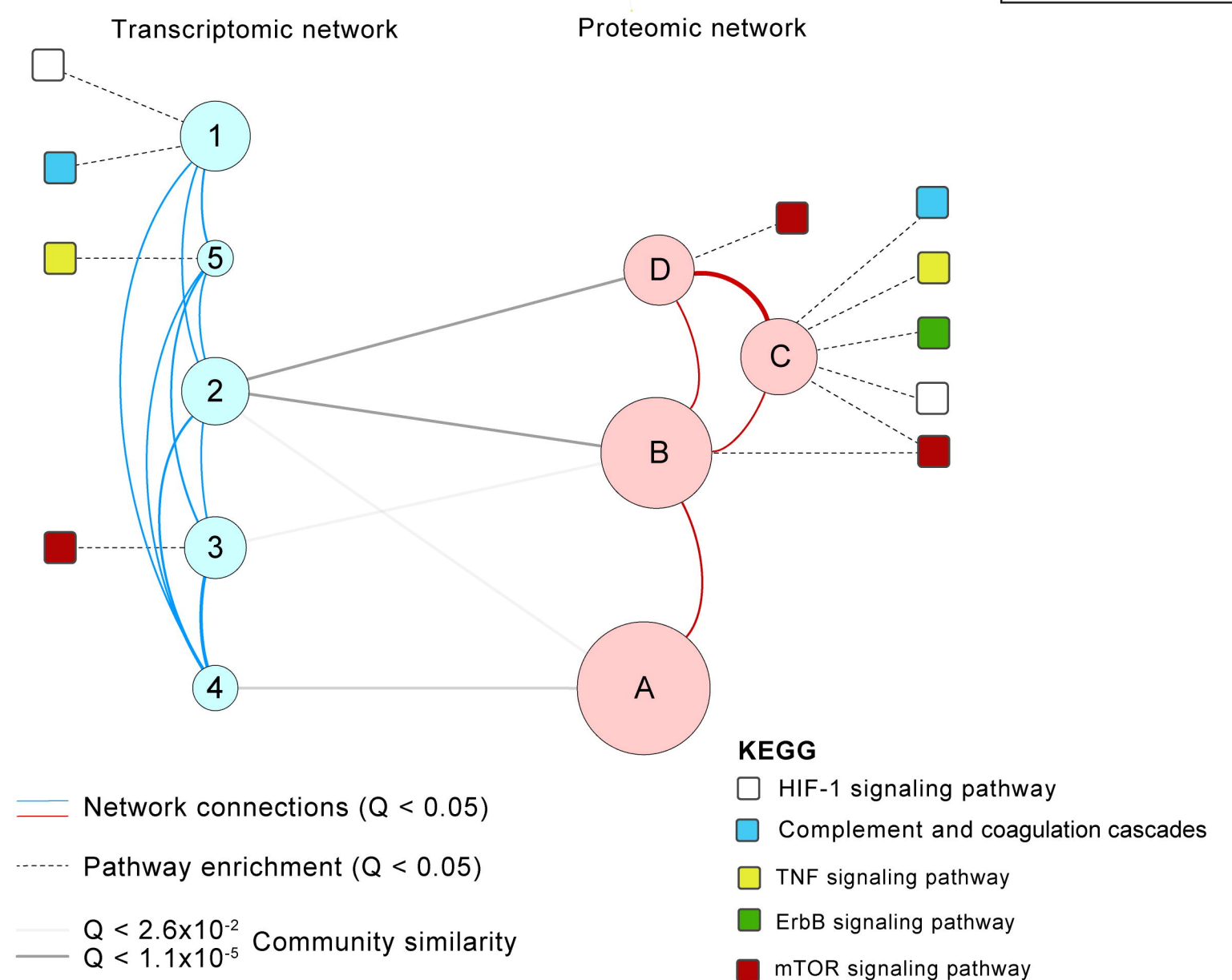


g.

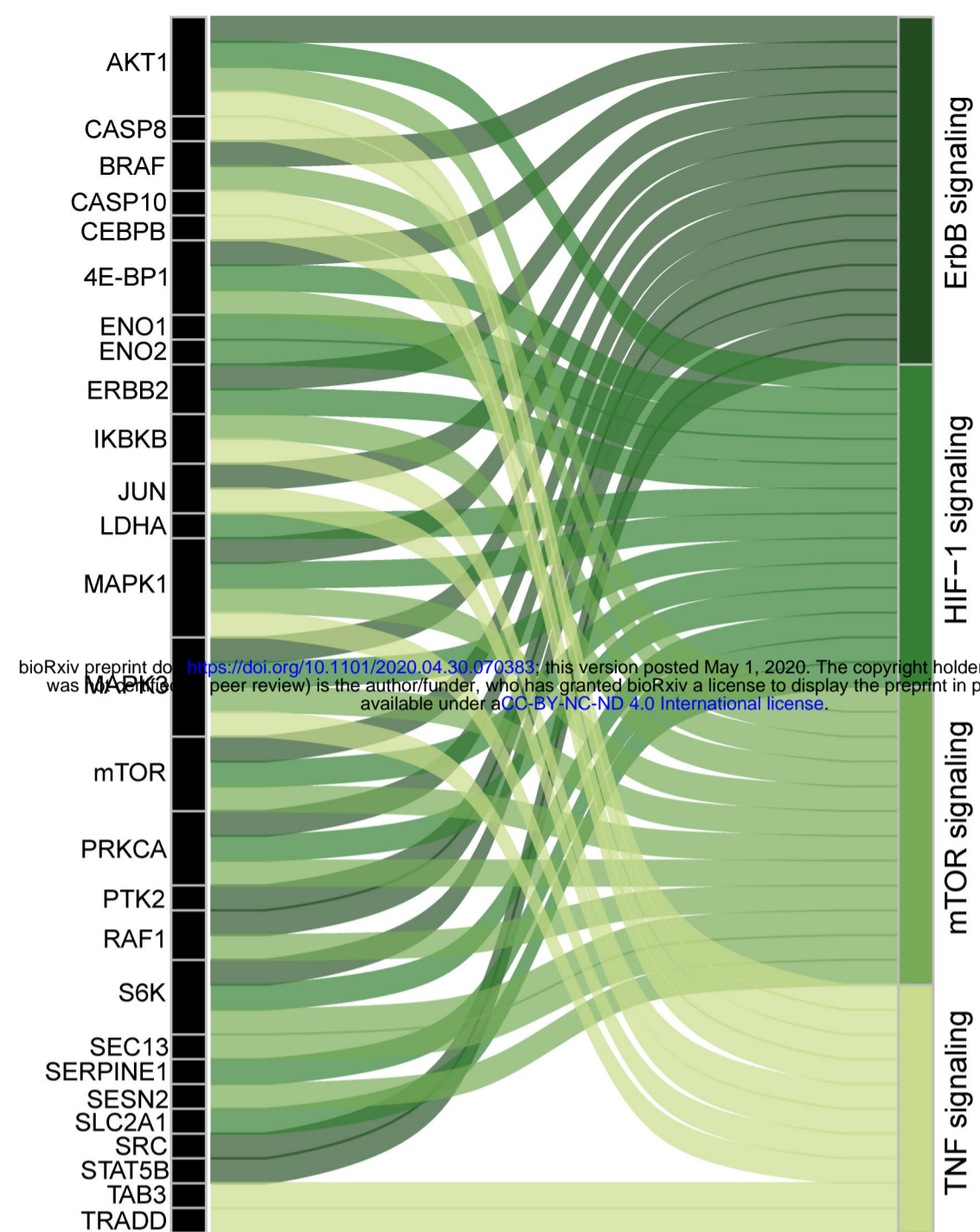
Proteomic network (Community D)



h.

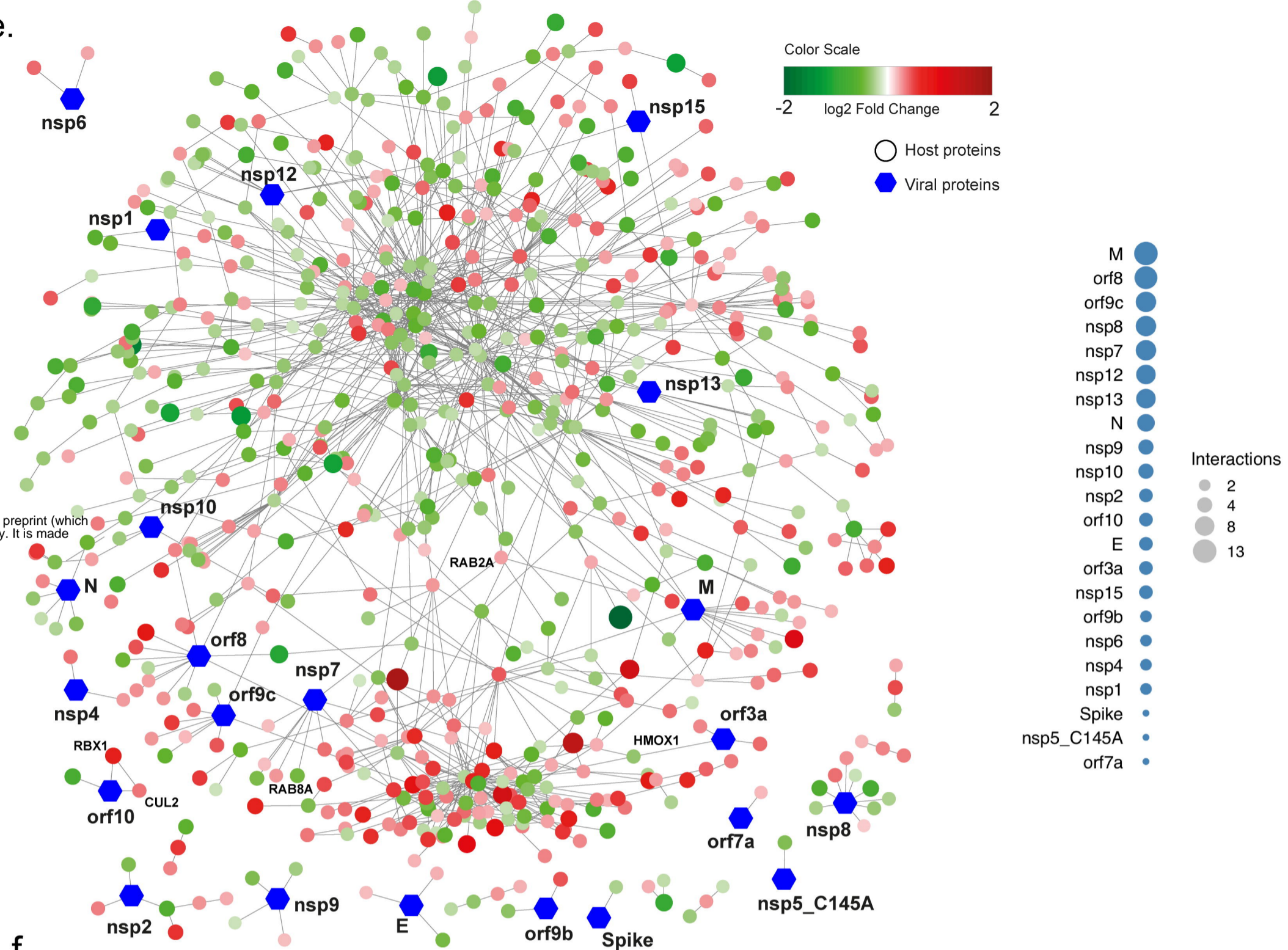


a.

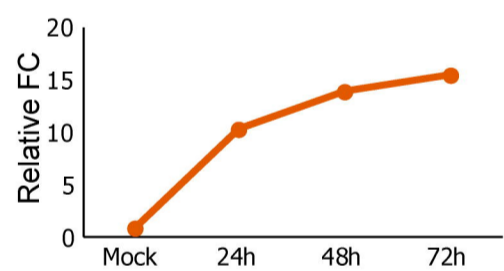


bioRxiv preprint doi: <https://doi.org/10.1101/2020.04.30.070383>; this version posted May 1, 2020. The copyright holder for this preprint (which was not certified by peer review) is the author/funder, who has granted bioRxiv a license to display the preprint in perpetuity. It is made available under aCC-BY-NC-ND 4.0 International license.

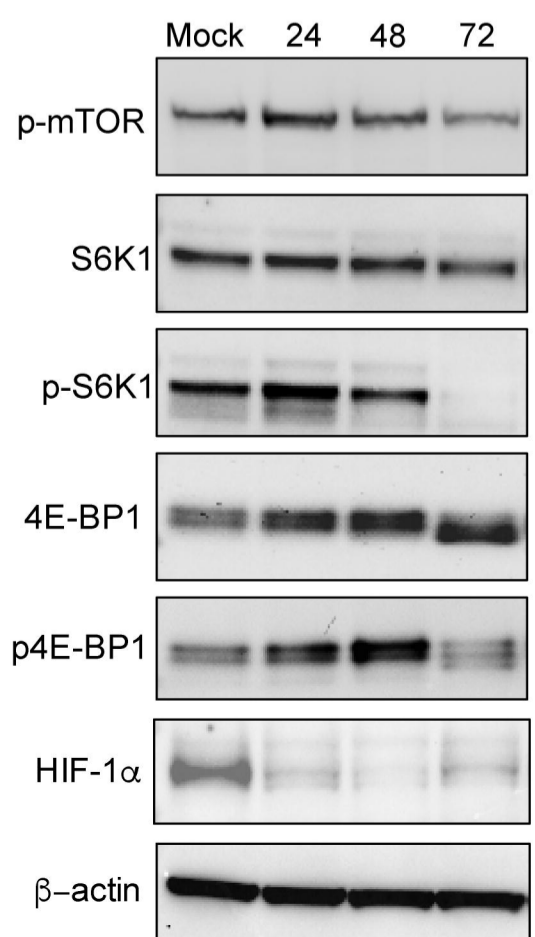
e.



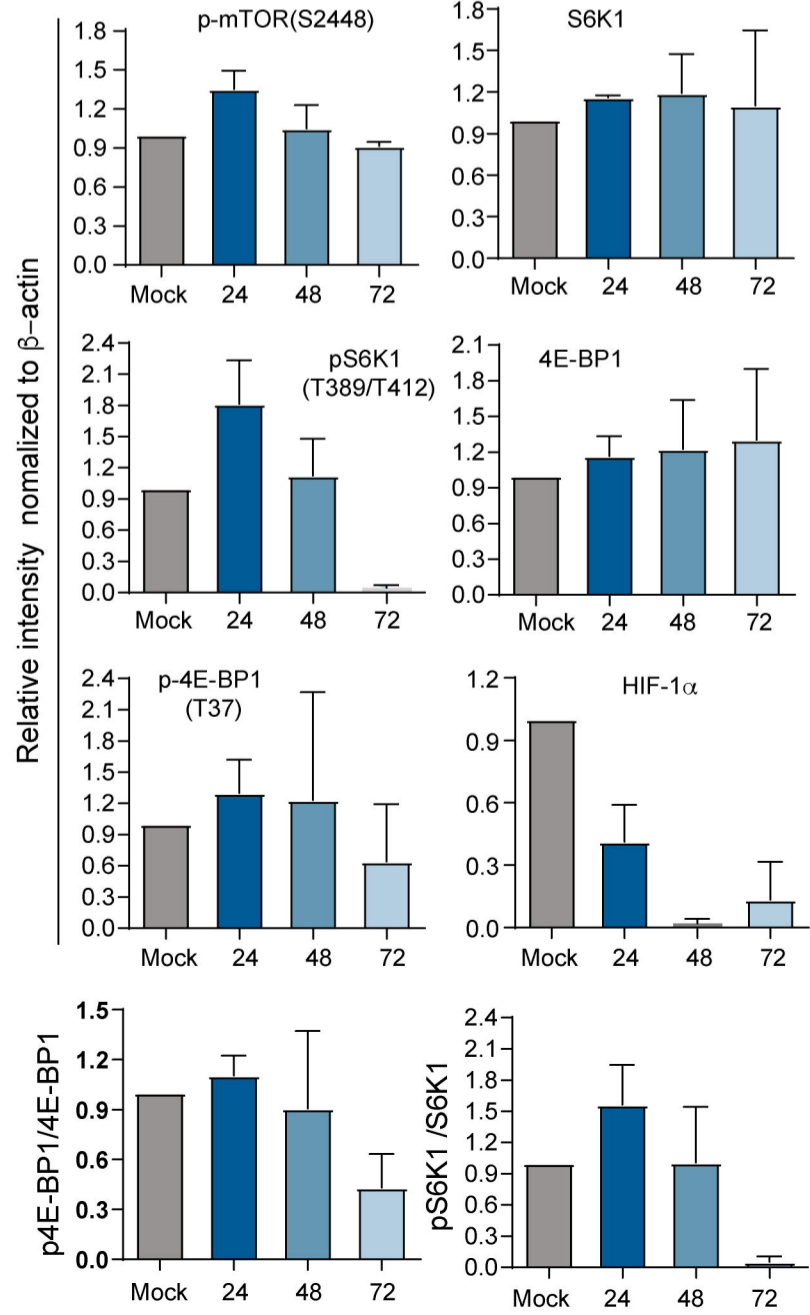
b.



c.



d.



f.

